

Suzaku measurement of electron and magnetic energy densities in the east lobe of the giant radio galaxy DA 240

Naoki ISOBE^{1,2}, Hiromi SETA³, & Makoto S. TASHIRO³

¹*Department of Astronomy, Kyoto University,*

Kitashirakawa-Oiwake-cho, Sakyo-ku, Kyoto 606-8502, Japan

²*Institute of Space and Astronautical Science (ISAS), Japan Aerospace Exploration Agency (JAXA)*

3-1-1 Yoshinodai, Chuo-ku, Sagami-hara, Kanagawa 252-5210, Japan

n-isobe@ir.isas.jaxa.jp

³*Department of Physics, Saitama University,*

255 Shimo-Okubo, Sakura-ku, Saitama, 338-8570, Japan

(Received 2011 March 23; accepted 2011 May 17)

Abstract

A careful analysis of the Suzaku data of the giant radio galaxy DA 240, of which the size is 1.48 Mpc, revealed diffuse X-ray emission associated with its east lobe. The diffuse X-ray spectrum was described with a simple power-law model with a photon index of $\Gamma = 1.92_{-0.17-0.06}^{+0.13+0.04}$, where the first and second errors represent the statistical and systematic ones. The agreement with the synchrotron radio photon index, $\Gamma_R = 1.95 \pm 0.01$ in 326 – 608.5 MHz, ensures that the excess X-ray emission is attributed to the inverse Compton emission from the synchrotron-radiating electrons, boosting up the cosmic microwave background photons. From the X-ray flux density, $51.5 \pm 3.9_{-5.4}^{+6.2}$ nJy at 1 keV derived with the photon index fixed at Γ_R , in comparison with the synchrotron radio intensity of 10.30 ± 0.12 Jy at 326 MHz, the magnetic and electron energy densities was estimated as $u_m = (3.0 \pm 0.2 \pm 0.4) \times 10^{-14}$ ergs cm⁻³ and $u_e = (3.4_{-0.2-0.4}^{+0.3+0.5}) \times 10^{-14}$ ergs cm⁻³ integrated over the electron Lorentz factor of $10^3 - 10^5$, respectively. Thus, the east lobe is found to reside in an equipartition condition between the electrons and magnetic field parametrized as $u_e/u_m = 1.1_{-0.1-0.2}^{+0.2+0.4}$. The east lobe of DA 240 is indicated to exhibit the lowest value of u_e , among all the X-ray detected lobes of radio galaxies. A comparison of the energetics in the giant radio galaxies with a size of ~ 1 Mpc to those in the smaller objects suggests a possibility that radio galaxies lose their jet power, as they evolve from ~ 100 kpc to ~ 1 Mpc.

1. Introduction

Among extragalactic radio source, those with a physical size larger than ~ 1 Mpc at the source rest frame are called as *giant radio galaxies*. The synchrotron aging technique suggests that they are relatively old sources with a typical age of ~ 100 Myr (Schoenmakers et al. 2000). Therefore, from the giant radio galaxies, we can explore the late phase of the evolution of the radio sources and the associated jets, which is not yet well understood.

The bulk kinetic energy, carried by the jets of a radio galaxy, is integrated within the lobes after it is randomized and converted into the particle and magnetic energies at its terminal hot spots. The lobes are regarded as an important indicator of the past activity of the jets. One of the most valuable tools to measure the electron and magnetic energies stored in the lobes is diffuse inverse Compton (IC) X-ray emission, where the cosmic microwave background (CMB) photons are up-scattered (Harris & Grindlay 1979; hereafter IC/CMB). Actually, the energetics in the lobes of numbers of radio galaxies are investigated from the diffuse X-ray emission which was naturally interpreted as the IC/CMB emission in the last two decades, with ROSAT (Feigelson et al. 1995), ASCA (e.g., Kaneda et al. 1995; Tashiro et al. 1998; Tashiro et al. 2001), Chandra (e.g., Isobe et al. 2002; Croston et al.

2005; Yaji et al. 2010) and XMM-Newton (e.g., Isobe et al. 2005; Isobe et al. 2006). These results indicate a dominance of the electron energy over the magnetic one by typically an order of magnitude in the lobes of radio galaxies (Isobe et al. 2011 for a summary). However, most of the sample is limited to the sources with a total dimension of $D \lesssim 500$ kpc, so far.

The X-ray Imaging Spectrometer (XIS; Koyama et al. 2007) onboard the Suzaku observatory (Mitsuda et al. 2007), in combination with the Hard X-ray Detector (HXD; Takahashi et al. 2007), opened a new window for the X-ray study of the lobes of radio galaxies (e.g., Tashiro et al. 2009), thanks to its low and stable instrumental background, which is crucial to investigate diffuse X-ray emission. With the Suzaku XIS, detections of the diffuse X-ray photons has subsequently been reported from the giant radio galaxies 3C 326 (Isobe et al. 2009) and 3C 35 (Isobe et al. 2011), and these X-rays were successfully attributed to be radiated via the IC/CMB process. Based on these results, Isobe et al. (2011) proposed a possibility that the current jet power of the giant radio galaxies are significantly lower than that of the smaller objects. This motivated us to make a systematic X-ray study of giant radio galaxies.

The giant radio galaxy DA 240 is located at a redshift of $z = 0.035661$ (Rines et al. 2000). It is optically classi-

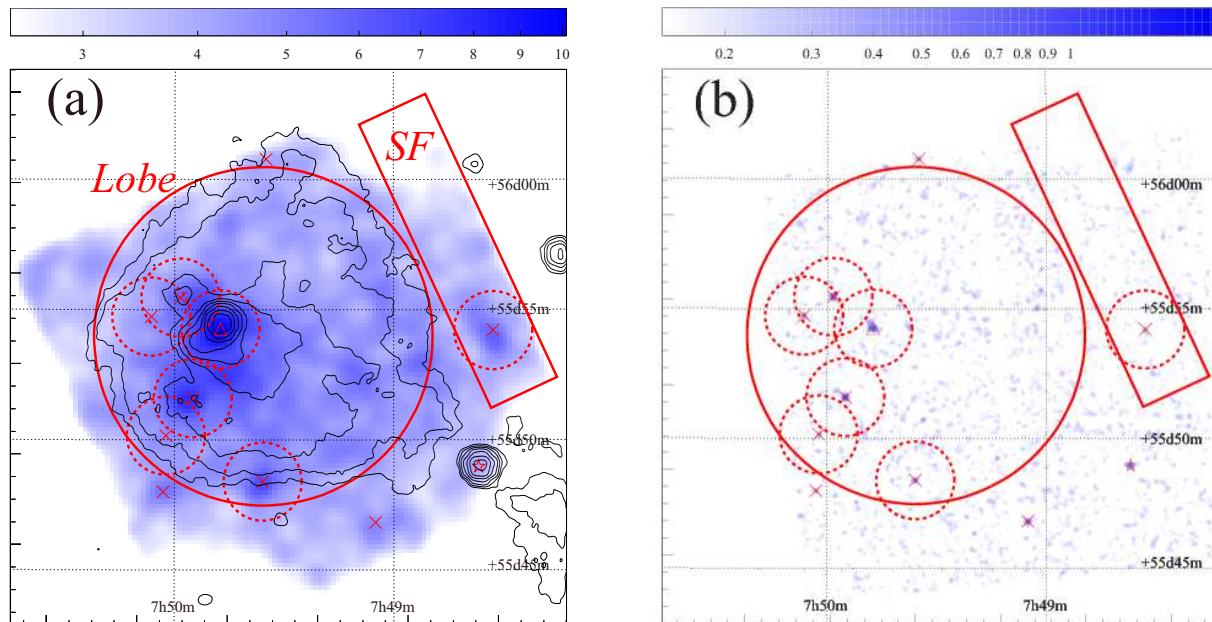


Fig. 1. (a) Suzaku XIS image of the east lobe of DA 240 in the 0.5 – 10 keV range, heavily smoothed with a two-dimensional Gaussian function of a $20''$ radius. The background events were not subtracted, while the exposure was not corrected. The scale bar on the top indicates the X-ray counts integrated within a $10'' \times 10''$ bin. A 608.5 MHz radio image (Leahy et al. unpublished) is superposed with contours. The Chandra position of the nucleus and hot spot are shown with the star and triangle, respectively. The other Chandra X-ray point sources, listed in table 1, are plotted with the crosses. The XIS events of the east lobe and XRB were accumulated within the solid circle denoted as **Lobe** and solid rectangle labeled as **SF**, respectively, with those in the dashed circles removed. (b) Chandra ACIS image of the same sky field in 0.3 – 10 keV, smoothed with a two-dimensional Gaussian function of a $4''$ radius. The scale bar displays the X-ray counts integrated within a $2'' \times 2''$ bin. The position of the Chandra X-ray sources and the spectral integration regions for the XIS are shown in the manner similar to that in panel (a).

fied into a low-excitation radio galaxy (Laing et al. 1983) with an elliptical host (Ebneter & Balick 1985). Its radio images (e.g., Mack et al. 1997) revealed its classical Fanaroff-Riley (FR) II morphology, where the lobes have a relatively flat brightness distribution. The total angular size of the source, $35'2''$, corresponds to a physical size of 1.48 Mpc at the redshift of the source. Its spectral age was estimated as 56 Myr (Strom et al. 1981), suggesting that it is a relatively old source. The object has a high integrated synchrotron radio flux of 9.2 Jy at 609 MHz (Mack et al. 1997), which suggests a high IC/CMB X-ray flux from its lobes. Although there is a bright radio hot spot in the east lobe, which was also detected in X-rays with XMM-Newton (Evans et al. 2008), its contamination to the lobe is to be estimated and to be clearly removed from the diffuse lobe emission owing to the large size of the lobe in comparison with the point spread function of the X-ray telescope (XRT; Serlemitsos et al. 2007) over the XIS with a half power diameter of $\sim 2'$ (Serlemitsos et al. 2007). These make DA 240 suitable for a Suzaku observation.

In the present paper, we adopted the cosmology with $H_0 = 71 \text{ km s}^{-1} \text{ Mpc}^{-1}$, $\Omega_m = 0.27$, and $\Omega_\lambda = 0.73$. These give the luminosity distance of 154.8 Mpc and the angle-to-size conversion ratio of $41.97 \text{ kpc}/1'$, at the redshift of DA 240 ($z = 0.035661$).

2. Observation and Data Reduction

2.1. Suzaku Observation

We performed a Suzaku observation of the giant radio galaxy DA 240, on 2010 March 19 – 21. We pointed the telescope at the east lobe, since its integrated radio flux is higher than that of the west lobe. In order to minimize the influence of the anomalous columns of XIS 0¹ and the hole of the optical blocking filter over XIS 1², the sky position with the J2000 coordinate of $(\alpha, \delta) = (117^\circ 3696', +55^\circ 8964')$ was placed at the XIS nominal position (Serlemitsos et al. 2007). As a result, the whole east lobe was observed within the clean field of view of the XIS. The normal clocking mode with no window option was adopted for the XIS while the normal mode was employed for the HXD.

We reduced the data with the latest version of the standard software package HEADAS 6.10. Since the lobe emission was found to be too faint for the HXD, only the XIS data are utilized. All the XIS data were reprocessed, by referring to the CALDB updated at 2010 July 30. We screened the data under the following standard criteria; the spacecraft is outside the south Atlantic anomaly (SAA), the time after an exit from the SAA is larger than 436 s, the geometric cut-off rigidity is higher than 6 GV,

¹ <http://www.astro.isas.jaxa.jp/suzaku/doc/suzakumemo/suzakumemo-2010-01.pdf>

² <http://www.astro.isas.jaxa.jp/suzaku/doc/suzakumemo/suzakumemo-2010-03.pdf>

Table 1. Chandra X-ray sources in the XIS field of view.

| (α, δ) | $\Delta\theta$ * | σ † | Source ID |
|--------------------------|------------------|------------|--------------|
| (117°:2709, +55°:7804) | 0.6 | 11.3 | |
| (117°:5127, +55°:8000) | 1.0 | 5.7 | |
| (117°:3994, +55°:8067) ‡ | 0.5 | 8.8 | |
| (117°:1535, +55°:8162) | 0.6 | 11.9 | The nucleus |
| (117°:5097, +55°:8360) ‡ | 1.1 | 5.7 | |
| (117°:4792, +55°:8600) ‡ | 0.5 | 17.3 | |
| (117°:1364, +55°:9035) § | 0.5 | 5.1 | |
| (117°:4477, +55°:9041) ‡ | 0.4 | 13.0 | The hot spot |
| (117°:5268, +55°:9122) ‡ | 0.9 | 6.7 | |
| (117°:4933, +55°:9244) ‡ | 0.4 | 14.0 | Ark 141 |
| (117°:3957, +56°:0130) | 1.0 | 5.8 | |

* Position error in arcsec.

† Source significance.

‡ Removed from the lobe spectrum.

§ Removed from the SF spectrum.

the source elevation above the rim of bright and night Earth is higher than 20° and 5° , respectively, and the XIS data are free from telemetry saturation. These yielded a good exposure of 75.5 ks. In the scientific analysis below, we selected the XIS events with a grade of 0, 2, 3, 4, or 6.

2.2. Archival Chandra Data

In order to identify possible contaminating faint X-ray sources unresolved with the XIS angular resolution, we analyzed the archival Chandra data. The sky field similar to that in the Suzaku observation was observed with the Chandra ACIS-I on 2009 January 12 (ObsID = 10237). The latest software package CIAO 4.3 was utilized in combination with CALDB 4.4.1. We reprocessed the ACIS data to create the new level 2 event file with the tool `chandra_repro`, following the standard manner. Because no significant background variation was found throughout the observation, no additional screening was performed to the new level 2 event file. As a result, a good exposure of 24.1 ks was derived. We adopted the grade selection same as for the XIS (i.e., 0, 2, 3, 4, or 6).

3. Results

3.1. X-ray image

The panel (a) of figure 1 displays the background-inclusive 0.5 – 10 keV Suzaku XIS image of the east lobe of DA 240, on which a 608.5 MHz radio image (Leahy et al., unpublished)³ is over-plotted with contours. We smoothed the XIS image with a two-dimensional Gaussian kernel of a $20''$ radius. The regions irradiated by the radioactive calibration source (^{55}Fe) on the corners of the XIS chips were removed, while the exposure correction was not performed. We noticed a systematic offset of $16.3''$ in the XIS coordinate determination, while this offset is found to be within the current systematic uncertainties (Uchiyama et al. 2008). We thus calibrated the XIS coor-

³ Taken from “An Atlas of DRAGNs”, edited by Leahy, Bridle, & Strom; <http://www.jb.man.ac.uk/atlas/>.

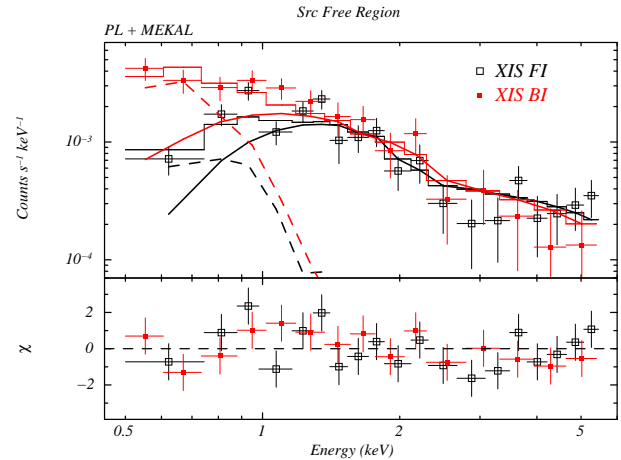


Fig. 2. Suzaku XIS spectrum of the SF region, fitted with the PL+MEKAL model. The solid and dashed lines indicate the PL and MEKAL components, respectively.

inate by ourselves, by referring to the Chandra position (see below) of the hot spot in the east lobe (the triangle in figure 1), which is clearly detected in the XIS image. After the coordinate correction, figure 1 indicates that the X-ray position of the hot spot deviates from its radio position by $\sim 10''$ toward the south direction. The similar positional offset, in addition to the detailed spatial structure of the hot spot, is reported by Evans et al. (2008), by using the higher-resolution radio and X-ray images obtained with the Very Large Array and XMM-Newton, respectively. We regard the detailed examination on this point is beyond the scope of the present paper.

Most of the east lobe was confirmed to be contained within the clean XIS field of view, while the nucleus of DA 240, indicated by the star in figure 1, was found to fall unfortunately on the XIS 0 anomalous columns. From the image alone, it is unclear whether or not diffuse faint X-ray emission associated with the lobe was detected.

The XIS image suggests several X-ray sources within the east lobe. Then, the Chandra ACIS image of the similar sky field in the 0.3 – 10 keV range is shown in figure 1 (b). The ACIS field of view is found to cover a large part of the east lobe. We made use of the CIAO tool `wavdetect` in order to pick up contaminating faint X-ray sources. Table 1 lists the detected X-ray sources with a significance higher than 5σ , among which the nucleus and hot spot of DA 240 were included. These sources are indicated on figure 1 with crosses.

3.2. X-ray background in the field

For the spectral analysis of diffuse and faint X-ray sources, it is of crucial importance to determine accurately the level of the X-ray background (XRB). Hence, we first evaluated the XRB spectrum in the field, from the source free (SF) region within the XIS field of view, which is displayed with the solid rectangle denoted as **SF** in figure 1. The region has a size of $12' \times 2'8$. Because figure 1 (b) reveals a faint X-ray source detected with the Chandra ACIS within the SF region (see table 1), we rejected a cir-

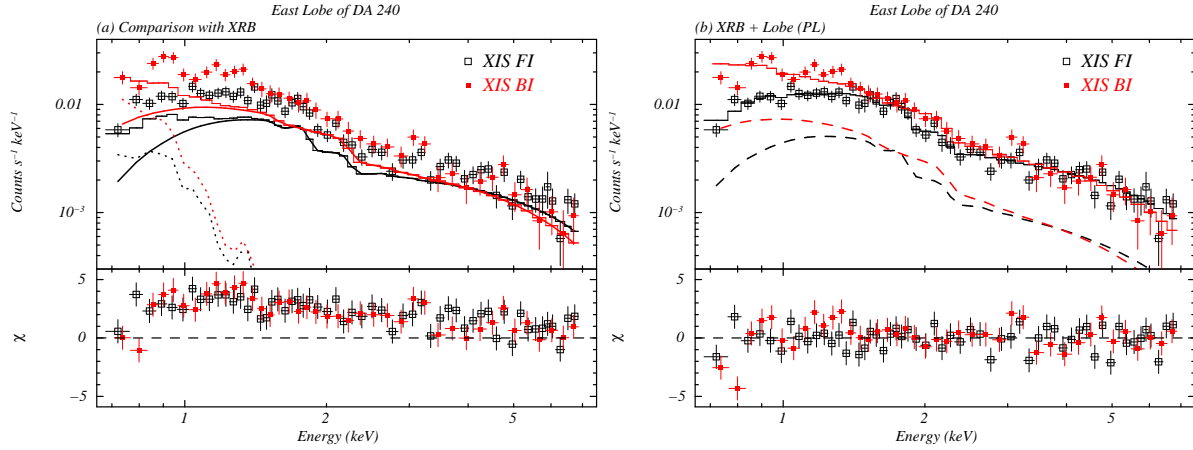


Fig. 3. Suzaku XIS spectrum of the east lobe of DA 240, accumulated from the Lobe region shown in figure 1. Panel (a) compares the data with the XRB model spectrum in the field of DA 240, determined from the SF region (figure 2 and table 2). The solid and dashed lines indicate the PL and MEKAL components, respectively. In panel (b), the best-fit model, in which the additional PL component (the dashed lines) describing the X-ray emission from the east lobe was taken into account. For clarity, the XRB model is omitted.

cle with a radius of $1'.5$ centered on the source (the dashed circle in figure 1). We confirmed that a source rejection with a larger radius yielded a similar result within the statistical uncertainties.

The non-X-ray background (NXB) in the region was estimated by the HEADAS tool `xisnxbgen`. The tool is reported to reproduce the NXB spectrum in the 1 – 7 keV range, with an accuracy better than $\sim 3\%$ for a typical exposure of 50 ks (Tawa et al. 2008). Figure 2 shows the NXB-subtracted XIS spectrum of the SF region. Although the region irradiated by the radioactive calibration source (^{55}Fe) in the north part of the SF region for the front-illuminated (FI) CCD chips (XIS 0 and 3; Koyama et al. 2007) was not removed, we limited the FI data below 5.5 keV.

Referring to Kushino et al. (2002) and Lumb et al. (2002), we approximate the XIS spectrum of the SF region with a composite model consisting of a hard power-law (PL) component and a soft thermal plasma emission described by the MEKAL (Mewe et al. 1985) code. The PL component is thought to be composed of unresolved faint X-ray sources, including distant active galactic nuclei, while the soft thermal emission is considered to be of Galactic origin. The PL photon index was fixed at $\Gamma = 1.41$ (Kushino et al. 2002), while the temperature of the thermal MEKAL component was left free and the solar abundance ratio was adopted. We assumed a common photoelectric absorption for both components with the Galactic hydrogen column density toward DA 240 ($N_{\text{H}} = 4.9 \times 10^{20} \text{ cm}^{-2}$; Kalberla et al. 2005). Response matrix functions (rmf) of the XIS was generated by the tool `xisrmfgen`. Assuming a uniform diffuse X-ray source with a $20'$ radius, we calculated the auxiliary response files (arf) by the tool `xissimarfgen` (Ishisaki et al. 2007).

We obtained an acceptable fit ($\chi^2/\text{dof} = 33.2/31$) by the PL+MEKAL model, as shown with the histograms in figure 2. The best-fit spectral parameters are summarized in table 2. The total absorption-inclusive surface

Table 2. Summary of the PL+MEKAL fitting to the XIS spectra of the SF region.

| Parameters | Values |
|--|--------------------------------|
| N_{H} (cm^{-2}) | $4.9 \times 10^{20} *$ |
| Γ | $1.41 \dagger$ |
| f_{PL} ($\text{ergs s}^{-1} \text{ cm}^{-2} \text{ str}^{-1}$) \ddagger | $(4.4 \pm 0.5) \times 10^{-8}$ |
| kT (keV) | $0.2_{-0.3}^{+0.6}$ |
| f_{th} ($\text{ergs s}^{-1} \text{ cm}^{-2} \text{ str}^{-1}$) \S | $(1.2 \pm 0.5) \times 10^{-8}$ |
| χ^2/dof | 33.2/31 |

* Fixed at the Galactic value (Kalberla et al. 2005).

† Taken from Kushino et al. (2002).

‡ Absorption-inclusive surface brightness of the PL component in 2 – 10 keV.

§ Absorption-inclusive surface brightness of the MEKAL component in 0.5 – 2 keV.

brightness of the XRB was measured as $f = 7.0_{-0.6}^{+0.5} \times 10^{-8} \text{ ergs s}^{-1} \text{ cm}^{-2} \text{ str}^{-1}$ in the 0.5 – 10 keV range. The MEKAL temperature derived as $kT = 0.20_{-0.03}^{+0.06} \text{ keV}$ is reasonable for the diffuse Galactic background emission ($kT = 0.204 \pm 0.009 \text{ keV}$; Lumb et al. 2002). The 2 – 10 keV surface brightness of the PL component, $f_{\text{PL}} = (4.4 \pm 0.5) \times 10^{-8} \text{ ergs s}^{-1} \text{ cm}^{-2} \text{ str}^{-1}$, was found to be consistent with the result in Kushino et al. (2002) within the 3σ uncertainty. Therefore, we decided to adopt the best-fit PL+MEKAL model for the XRB spectrum to the east lobe of DA 240.

3.3. X-ray spectrum of the east lobe

We extracted the XIS spectrum of the east lobe of DA 240, from the solid circle denoted as **Lobe** in figure 1 with a radius of $6'.5$ (corresponding to 272.8 kpc at the redshift of DA 240). The contamination from the Chandra X-ray sources within the Lobe region, tabulated in table 2, was removed, by rejecting the dashed circles in figure 1, all of which has a radius of $1.5'$. Figure 3 shows the XIS spectrum of the Lobe region in the range of 0.7 –

Table 3. Summary of signal statistics in the 0.7 – 7 keV range

| Region | Component | FI rate (cts s ⁻¹) | BI rate (cts s ⁻¹) | F_X (ergs s ⁻¹ cm ⁻²) * |
|-----------|-----------|--|--|--|
| Lobe | Data | $(3.81 \pm 0.05) \times 10^{-2}$ | $(5.62 \pm 0.09) \times 10^{-2}$ | |
| | NXB † | $(1.36 \pm 0.01 \pm 0.04) \times 10^{-2}$ | $(2.35 \pm 0.02 \pm 0.07) \times 10^{-2}$ | |
| | XRB | $(1.63_{-0.10}^{+0.09}) \times 10^{-2}$ | $(2.09_{-0.13}^{+0.10}) \times 10^{-2}$ | $(4.9 \pm 0.5) \times 10^{-12}$ ‡ |
| | Signal † | $(0.83 \pm 0.05_{-0.10}^{+0.11}) \times 10^{-2}$ | $(1.18 \pm 0.09_{-0.13}^{+0.15}) \times 10^{-2}$ | $(2.9 \pm 0.2_{-0.3}^{+0.4}) \times 10^{-13}$ § |
| hot spot | | $(1.77 \pm 0.21) \times 10^{-3}$ | $(1.82 \pm 0.23) \times 10^{-3}$ | $(5.3 \pm 0.5) \times 10^{-14}$ |
| nucleus # | — | | $< 5.6 \times 10^{-4}$ | $< 2.7 \times 10^{-14}$ ** |

* Absorption-inclusive 0.7 – 7 keV flux

† The first and second errors represent the statistical and systematic ones, respectively.

‡ Normalized to the sky region with a radius of 20 arcmin, based on the best-fit PL+MEKAL spectrum (table 2).

§ Evaluated from Case 1 in table 4.

|| Evaluated from the best-fit PL spectrum (table 5).

The 3 σ BI upper limit is shown.

** A PL spectrum with a photon index of $\Gamma = 1.91$ (Evans et al. 2008), modified by the Galactic absorption, is assumed.

7 keV, after the NXB, evaluated by the `xisnxbgen`, was subtracted. The signal statistics within the Lobe region are summarized in table 3. The 0.7 – 7 keV data count rate per CCD chip was measured as $(3.81 \pm 0.05) \times 10^{-2}$ cts s⁻¹ and $(5.62 \pm 0.09) \times 10^{-2}$ cts s⁻¹ with the XIS FI and BI, respectively, while the NXB count rate was estimated as $(1.36 \pm 0.01) \times 10^{-2}$ cts s⁻¹ and $(2.35 \pm 0.02) \times 10^{-2}$ cts s⁻¹. Here, the 1 σ statistical errors are accompanied with the value. We, thus, confirmed the NXB-subtracted X-ray signals of $(2.46 \pm 0.05) \times 10^{-2}$ cts s⁻¹ and $(3.27 \pm 0.09) \times 10^{-2}$ cts s⁻¹, yielding the statistical significance of 48.2 σ and 37.2 σ , with the XIS FI and BI, respectively. In addition, these signals are found to well exceed the typical systematic NXB fluctuation of $\sim 3\%$ (Tawa et al. 2008), which corresponds to the FI and BI count rates of 0.04×10^{-2} cts s⁻¹ and 0.07×10^{-2} cts s⁻¹ respectively.

In panel (a) of figure 3, we compare the NXB-subtracted XIS spectrum of the Lobe region with the XRB in the field. The best-fit PL+MEKAL model of the XRB determined from the SF region (figure 2 and table 2) was convolved with the `rmf` and the `arf` for the Lobe region, created in the manner similar to those of the SF region, and plotted with the solid (PL) and dotted (MEKAL) lines. The XRB model, convolved with the `rmf` and `arf`, yields a 0.7 – 7 keV FI and BI count rate of $(1.63_{-0.10}^{+0.09}) \times 10^{-2}$ cts s⁻¹ and $(2.09_{-0.13}^{+0.10}) \times 10^{-2}$ cts s⁻¹, respectively. As a result, we have securely detected excess signals above the XRB level with an FI and BI count rate of $(0.83 \pm 0.05_{-0.10}^{+0.11}) \times 10^{-2}$ cts s⁻¹ and $(1.18 \pm 0.09_{-0.13}^{+0.15}) \times 10^{-2}$ cts s⁻¹ respectively. Here, the first error represents the statistical error, while the second error takes into account the error from the XRB model and the systematic error from the NXB. The residual χ -spectrum in panel (a) of figure 1 clearly visualizes the significance of the excess ($\chi^2/\text{dof} = 594.9/97$ in 0.7 – 7 keV).

We reproduced the excess emission from the east lobe by an additional PL component, subjected to the Galactic absorption ($N_H = 4.9 \times 10^{20}$ cm⁻²). In order to create the `arf` for the lobe, we assumed a uniform emission filling a circle with a radius of 7 arcmin (293.8 kpc at the source rest frame), referring to the 608 MHz radio image shown

Table 4. Best-fit spectral parameters for the excess X-ray emission from the east lobe.

| Parameters | Case 1 | Case 2 |
|---------------------------|----------------------------------|------------------------------|
| N_H (cm ⁻²) | | 4.9×10^{20} * |
| Γ ‡ | $1.92_{-0.17-0.06}^{+0.13+0.04}$ | 1.95 † |
| $S_{1\text{keV}}$ (nJy) ‡ | $50.7_{-5.6-4.7}^{+4.7+5.3}$ | $51.5 \pm 3.9_{-5.4}^{+6.2}$ |
| χ^2/dof | 117.6/95 | 117.9/96 |

* Fixed at the Galactic value (Kalberla et al. 2005).

† Fixed at the radio index (Mack et al. 1997).

‡ The first and second errors represent the statistical and systematic ones, respectively.

in figure 1. As shown in panel (b) of figure 3, a reasonable fit ($\chi^2/\text{dof} = 117.6/95$) was derived by the additional PL component with the parameters summarized in table 4 (Case 1). The photon index, $\Gamma = 1.92_{-0.17-0.06}^{+0.13+0.04}$, was found to be fairly consistent with that of the low-frequency synchrotron radio spectrum in the range of 326 – 608.5 MHz, $\Gamma_R = 1.95$ (Mack et al. 1997). Here the first error is due to the photon statistics of the spectrum, while the second one is propagated from the systematic errors of both NXB and XRB. When the photon index was fixed at the radio index (Case 2), we measured the 1 keV flux density of the additional PL component as $S_{1\text{keV}} = 51.5 \pm 3.9_{-5.4}^{+6.2}$ nJy.

3.4. X-ray spectra of the hot spot and nucleus

The X-ray signals were accumulated from the circle with a radius of 1' centered on the Chandra position of the hot spot. The background was estimated from the 2' circle within the lobe, free from the X-ray point sources (shown in table 1). The background-subtracted XIS spectrum of the east hot spot of DA 240 is shown in figure 4, and the signal statistics are presented in table 3. The `arf` for a point source at the position of the hot spot is calculated with `xissimarfgen`. We successfully described the observed spectrum with a simple PL model, modified with the Galactic absorption, and tabulate the best-fit parameters in table 5. Both the photon index ($\Gamma = 1.99_{-0.27}^{+0.28}$) and 1 keV flux density ($S_{1\text{keV}} = 9.9 \pm 1.8$ nJy) are found to be consistent within the statistical uncertainties, with

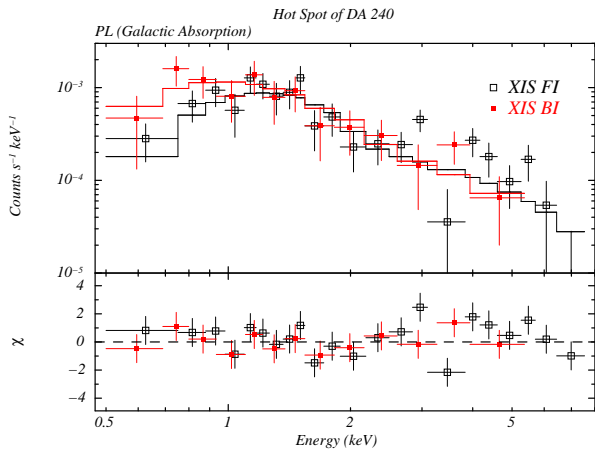


Fig. 4. Suzaku XIS spectrum of the east hot spot of DA 240, which is successfully fitted with a simple PL model subjected to the Galactic absorption toward DA 240.

the XMM-Newton result ($\Gamma = 2.2 \pm 0.3$ and $S_{1\text{keV}} = 7 \pm 1$ nJy; Evans et al. 2008).

In the similar manner, the XIS signals from the nucleus of DA 240 was integrated within the circle with a $1'$ radius centered on it, while the background was derived from a neighboring point-source-free region with a $2'$ radius. As we briefly stated in §3.1, the anomalous columns of XIS 0 intersect the source region. In addition, the nucleus is found to be unfortunately located at the boundary of the calibration source region for XIS 3. These are possible to make a significant impact on a faint source. Therefore, we decided to utilize only the XIS 1 (i.e., BI) data for the nucleus. As is shown in table 3, we found that the nuclear XIS BI signals are statistically insignificant with a 3σ upper limit on the $0.7 - 7$ keV BI count rate of 5.6×10^{-4} cts s^{-1} . With the point source at the position of the nucleus, this is converted to the upper limit on the absorption-inclusive X-ray flux and luminosity at the source frame of 2.7×10^{-14} ergs s^{-1} and 8.0×10^{40} ergs s^{-1} in the $0.7 - 7$ keV range, when we adopt the PL spectrum absorbed by the Galactic column density with a photon index of $\Gamma = 1.91$, which is reported from the XMM-Newton observation of the DA 240 nucleus conducted on 2006 October 18 (Evans et al. 2008). The $2 - 10$ keV X-ray intrinsic luminosity of 5.5×10^{40} ergs s^{-1} determined from the XMM-Newton spectrum, which corresponds to the $0.7 - 7$ keV absorption-inclusive luminosity of 7.1×10^{40} ergs s^{-1} , is found to be consistent with the Suzaku upper limit. Thus, we detected no evidence of a significant intensity variation between the two observations, separated by ~ 3.4 years from each other.

4. Discussion

4.1. Energetics in the east lobe of DA 240

With the careful subtraction of the XRB, NXB and contaminating X-ray point sources from the Suzaku XIS data, we have revealed the significant X-ray emission from the east lobe of the giant radio galaxy DA 240. We also

Table 5. Best-fit spectral parameters for the hot spot.

| Parameters | Values |
|-------------------------------------|------------------------|
| N_{H} (cm^{-2}) | 4.9×10^{20} * |
| Γ | $1.99^{+0.28}_{-0.27}$ |
| $S_{1\text{keV}}$ (nJy) | 9.9 ± 1.8 |
| χ^2/dof | 34.3/33 |

* Fixed at the Galactic value (Kalberla et al. 2005).

detected the hot spot within the east lobe, of which the XIS spectrum is reproduced by a PL model with a photon index of $\Gamma = 1.99^{+0.28}_{-0.27}$ and a 1 keV flux density of $S_{1\text{keV}} = 9.9 \pm 1.8$ nJy), although the nucleus was found to be too faint with an upper limit on the $0.7 - 7$ keV observed luminosity of 8.0×10^{40} ergs s^{-1} .

The XIS spectrum of the lobe was successfully described by a PL model with a photon index of $\Gamma = 1.92^{+0.13+0.04}_{-0.17-0.06}$. We plotted the radio and X-ray spectral energy distribution of the east lobe in figure 5. Here, we note that the contribution from the hot spot was not subtracted from the radio data. The high-frequency spectrum in the $4.8 - 10.6$ GHz range appears to be hard with a photon index of $\Gamma_{\text{R}} = 1.58 \pm 0.01$ (Mack et al. 1997), since the hot spot is dominant in the range. In contrast, the lobe exhibits a steep spectral index, $\Gamma_{\text{R}} = 1.95 \pm 0.01$ in the $326 - 608.5$ MHz, where the contamination from the hot spot becomes unimportant (Mack et al. 1997). The agreement between the radio synchrotron and X-ray spectral slopes of the lobe, in combination with the fact that the radio and X-ray spectra do not smoothly connect to each other as we see in figure 5, strongly supports the interpretation that the synchrotron electrons in the east lobe radiate the excess X-ray emission through the IC scattering. Such IC X-ray emission is widely observed from other radio sources (e.g., Croston et al. 2005), including giant radio galaxies (e.g., Isobe et al. 2009; Isobe et al. 2011).

We evaluate the energy density of the possible seed photon candidates for the IC process in the lobe. These include the CMB photons (Harris & Grindlay 1979), infrared (IR) radiation from the active nucleus (Brunetti et al. 1997), and the synchrotron photons produced within the lobe themselves. Assuming an isotropic radiation, the IR flux density of the DA 240 nucleus, 53 mJy at $60 \mu\text{m}$ (Golombek et al. 1998), yields an IR photon energy density of $\sim 2 \times 10^{-16} (r/100 \text{ kpc})^{-2}$ ergs cm^{-3} where r is the distance from the nucleus. In the case of the FR II radio galaxies, including DA 240, IR photons from the base of the jet could serve as a seed photon source to some extent. Since a large part of such IR emission is thought to be unobservable from our line of sight, due to a beaming effect from the relativistic bulk motion of the jet, it is not easy to evaluate precisely its energy density. Assuming a typical Doppler beaming factor of $\delta \sim 10$ (e.g., Inoue & Takahara 1996), the IC scattering off the jet IR photons is thought to become effective only within the narrow cone toward the jet direction with an opening angle of $\sin \theta \sim 1/10$. If this is the case, the IC X-ray emission should be en-

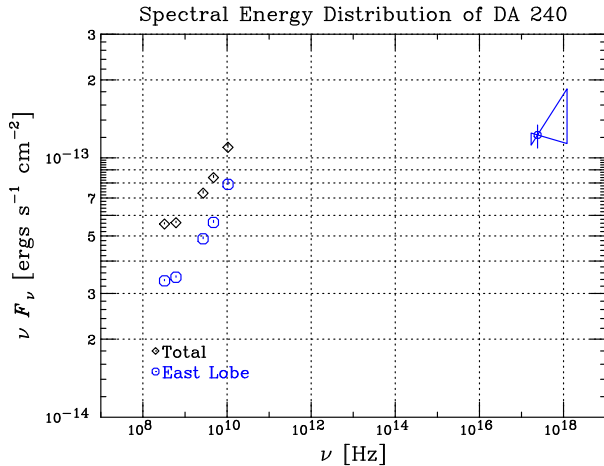


Fig. 5. Spectral energy distribution of the east lobe of DA 240. The synchrotron radio data (Mack et al. 1997) of the whole radio source and east lobe were plotted by the diamonds and circles, respectively. The best-fit PL component to the excess X-ray emission from the lobe was shown with the bow tie.

hanced along the jet, connecting the nucleus and hot spot. However, we do not find such spatial structure in the XIS image in figure 1. Therefore, we regard that such IC process is unimportant for the X-ray emission observed from the lobe of DA 240. From the radio spectrum plotted in figure 5, the synchrotron photons are estimated to be negligible, with an energy density of $\ll 10^{-18}$ ergs cm^{-3} if it is spatially averaged over the lobe. Thus, we concluded that the CMB, with an energy density of $u_{\text{CMB}} = 4.7 \times 10^{-13}$ ergs cm^{-3} at the redshift of DA 240 ($z = 0.035661$), highly dominates the other seed photon sources. The recent γ -ray result with Fermi from Centaurus A (Abdo et al. 2010) confirmed an additional contribution from the extragalactic background light to the seed photon source. However, such IC emission is only detectable at the highest energy end of the IC spectrum in the GeV γ -ray range with only a negligible X-ray flux.

Based on the simple analytical formula for the IC/CMB process presented in Harris & Grindlay (1979), we derive the energy densities of the electrons and magnetic field, u_e and u_m respectively, in the east lobe of DA 240. The low-frequency radio synchrotron flux density and photon index was adopted from Mack et al. (1997) as $S_{\text{R}} = 10.30 \pm 0.12$ Jy at 326 MHz and $\Gamma_{\text{R}} = 1.95 \pm 0.01$ in 326 – 608.5 MHz. Correspondingly, the electron number density spectrum was assumed to be a simple PL form as $\propto \gamma_e^{-p}$ with $p = 2\Gamma_{\text{R}} - 1 = 2.9$, where γ_e is the electron Lorentz factor. The IC/CMB X-ray flux density was measured from the PL fitting with the photon index fixed at this radio index, as $S_{1\text{keV}} = 51.5 \pm 3.9_{-5.4}^{+6.2}$ nJy (Case 2 in table 4). From the 608.5 MHz radio image shown in figure 1, we approximate the shape of the lobe at a simple sphere with a radius of 293.8 ± 4.2 kpc (corresponding to $7' \pm 0.1$), which gives a volume of $V = (3.13 \pm 0.13) \times 10^{72}$ cm^3 . The filling factor of the electron and magnetic field in the lobe were supposed to be unity.

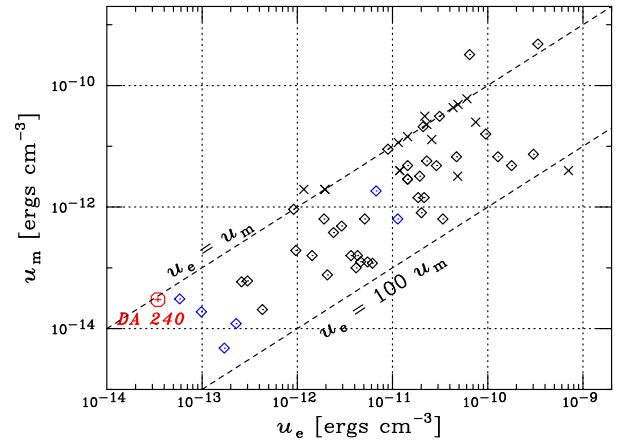


Fig. 6. Summary of u_e and u_m in lobes of radio galaxies (Croston et al. 2005; Isobe et al. 2011; Konar et al. 2010, and reference therein). The east lobe of DA 240 is indicated by the red circle, with the statistical error. The lobes, from which the significant IC X-ray detection was reported, are plotted with diamonds, while those with only the upper limit on the IC flux are shown with crosses. The giant radio galaxies are shown with the blue symbols. The two dashed lines represent the equipartition and a particle dominance of $u_e/u_m = 1$, and 100, respectively.

The energetics in the east lobe of DA 240 are summarized in table 6, together with the input quantities discussed above. The energy densities of electrons and magnetic field were evaluated as $u_e = (3.4_{-0.2-0.4}^{+0.3+0.5}) \times 10^{-14}$ ergs cm^3 and $u_m = (3.0 \pm 0.2 \pm 0.4) \times 10^{-14}$ ergs cm^3 , respectively; the latter of which corresponds to the magnetic field of $B = 0.87 \pm 0.03_{-0.06}^{+0.05}$ μG . Here, the first error represents the statistical error from $S_{1\text{keV}}$, while the second one takes into account all the possible systematics from $S_{1\text{keV}}$, S_{R} , α_{R} and V . We have confirmed an energy equipartition between the electrons and magnetic field as $u_e/u_m = 1.1_{-0.1-0.2}^{+0.2+0.4}$.

4.2. Implication on the evolution of the lobe energetics

In figure 6 (Croston et al. 2005; Isobe et al. 2011; Konar et al. 2010 and reference therein), we compiled the relation between u_e and u_m in the lobes of radio galaxies, disentangled with the IC/CMB technique. Giant radio galaxies (shown with the blue symbols) tend to be distributed around the bottom-left corner in the diagram, except for the lobes of 3C 457 (Konar et al. 2010) of which the data point is located around the center of the distribution. Especially, u_e in the east lobe of DA 240 is measured to be the lowest among all the X-ray detected lobes. In addition, u_m in the giant radio galaxies is typically indicated to be lower than than the CMB energy density. Thus, this result strengthened the idea that the dominance of the IC/CMB radiative losses over the synchrotron one is a common properties in the lobes of giant radio galaxies (Ishwara-Chandra & Saikia 1999).

As we frequently pointed out in the previous paper (e.g., Isobe et al. 2005; Isobe et al. 2009; Isobe et al. 2011), the lobes typically exhibit an electron dominance of $u_e/u_m \sim 10$, over a wide range of u_e and u_m . In con-

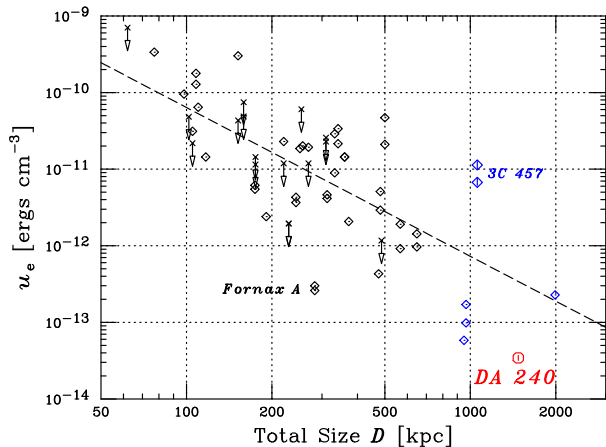


Fig. 7. Electron energy density u_e in the lobes, plotted against the total physical size D of the radio galaxies. The east lobe of DA 240 is indicated with the red circle, while the other giant radio galaxies are plotted with the blue diamonds. The dashed line shows the best-fit u_e - D relation except for the giant radio galaxies.

trast, a relatively large fraction of the giant radio galaxies detected with the IC/CMB X-rays (DA 240 and 3C 35 out of the 5 giants in total) is found to reside nearly in the equipartition condition. We speculate that as the radio source develops from a $\lesssim 100$ kpc scale to a Mpc one, the energetics in their lobes evolve from the electron dominance to the equipartition, in addition to a significant decrease in both u_e and u_m .

The evolution of the lobe energetics is more explicitly examined in figure 7, which plots the relation between u_e and the total size D of the radio galaxies. It is pointed out that a radio galaxy develops along the relation of $u_e \propto D^{-2}$ while its lobes are actively energized by its jets (Isobe et al. 2009; Isobe et al. 2011). After the jet power supplied to the lobes becomes declined, the value of u_e is thought to be significantly reduced by adiabatic expansion and radiative losses due to synchrotron and IC/CMB emission. This idea is supported by a correlation of $u_e \propto D^{-1.9 \pm 0.4}$ for the radio galaxies with $D < 900$ kpc (the black diamonds), which is shown with the dashed line in figure 7. On the other hand, it is notable that for the radio galaxy with a dormant nucleus, Fornax A (Iyomoto et al. 1998), the data points are located below the correlation line by more than an order of magnitude in figure 7 (Isobe et al. 2006; Tashiro et al. 2009).

Interestingly, the giant radio galaxies also tend to exhibit a lower value of u_e compared with the u_e - D relation for those with $D < 900$ kpc. This implies a significant decrease in the jet activity of radio galaxies, in the range of $D = 100$ kpc–1 Mpc. Even though the bright radio hot spots in DA 240 suggesting an ongoing energy input to its lobes, the relatively steep synchrotron radio and IC X-ray spectra with the photon index of $\Gamma \sim 1.95$ indicate that the east lobe of this radio galaxy resides in a strong cooling regime. This means that the current energy supply to the lobe is ineffective, in comparison with the cooling loss. In fact, the rather inactive nucleus of DA 240, re-

vealed in the XMM-Newton observation with an observed luminosity of 7.1×10^{40} ergs s^{-1} and re-confirmed in this Suzaku observation with the upper-limit X-ray luminosity of 8.0×10^{40} ergs s^{-1} in the 0.7–7 keV range, is thought to be compatible with the currently low power jet scenario.

In figures 6 and 7, we found an outlier among the giant radio galaxies, 3C 457, with exceptionally high energy densities of $u_e \sim 10^{-11}$ ergs s^{-1} and $u_m \sim 10^{-12}$ ergs s^{-1} (Konar et al. 2010), which are comparable to those of the “normal” radio galaxies with $D \sim 200$ kpc. It is reported that 3C 457 hosts a rather active nucleus with a 0.7–7 keV intrinsic luminosity of $\sim 4 \times 10^{44}$ ergs s^{-1} (estimated from Konar et al. 2010), which is more than 3 orders of magnitude higher than that of DA 240. Since its radio images revealed bright hot spots at the edge of the individual lobes (Konar et al. 2010), it is concluded that the lobes of 3C 457 are currently expanding very fast. These are naturally regarded to be equivalent to the ongoing energy input to the lobes from the jets through the hot spots, in this radio galaxy. These active features of 3C 457 are thought to be related to the fact that the source is relatively young with a spectral age of ~ 30 Myr (Konar et al. 2010) as a giant radio galaxy (typically ~ 100 Myr; Schoenmakers et al. 2000).

Finally, based on the consideration above, we have proposed that the jet of typical radio galaxies is possible to reduce its activity, as they evolve in size typically from $D \sim 100$ kpc to $D \sim 1$ Mpc, although the number of giant radio galaxies, studied with the IC/CMB X-ray emission, is still small. In order to make a definite conclusion, X-ray observations of giant radio galaxies are strongly encouraged with Suzaku and future high-sensitivity X-ray missions, including the next generation Japanese X-ray observatory ASTRO-H (Takahashi et al. 2010).

We are grateful to all the members of the Suzaku team, for the successful operation and calibration. We thank the referee for her/his kindness to improve the paper. This research has made use of the archival Chandra data and its related software provided by the Chandra X-ray Center (CXC). The support is acknowledged from the Ministry of Education, Culture, Sports, Science and Technology (MEXT) of Japan through the Grant-in-Aid for the Global COE Program, “The Next Generation of Physics, Spun from Universality and Emergence”. This investigation is partially supported by the MEXT Grant-in-Aid for Young Scientists (B) 22740120 (N. I.) and for Scientific Research (B) 22340039 (M. S. T.).

References

- Abdo, A.A., et al., 2010, *Science*, 328, 725
- Brunetti, G., Setti, G., & Comastri, A., 1997, *A&A*, 325, 898
- Croston, J. H., Hardcastle, M. J., Harris, D. E., Belsole, E., Birkinshaw, M., & Worrall, D. M., 2005, *ApJ*, 626, 733
- Ebner, K., & Balick, B., 1985, *AJ*, 90, 183
- Evans, D. A., Hardcastle, M. J., Lee, J. C., Kraft, R. P., Worrall, D. M., Birkinshaw, M., & Croston, J. H., 2008, *ApJ*, 688, 844
- Feigelson, E. D., Laurent-Muehleisen, S. A., Kollgaard, R. I., & Fomalont, E. B., 1995, *ApJ*, 449, L149

Table 6. Summary of the energetics in the DA 240 east lobe.

| Parameters | Values | Comment |
|---|---------------------------------|-----------------------------------|
| $S_{1\text{keV}}$ (nJy) | $51.5 \pm 3.9^{+6.2}_{-5.4}$ | Case 2 |
| S_{R} (Jy) | 10.24 ± 0.1 | 326 MHz |
| Γ_{R} | 1.95 ± 0.01 | 326 – 608.5 MHz |
| V (10^{72} cm ³) | 3.13 ± 0.13 | |
| u_{e} (10^{-14} ergs cm ⁻³) * | $3.4^{+0.3+0.5}_{-0.2-0.4}$ | $\gamma_{\text{e}} = 10^3 - 10^5$ |
| u_{m} (10^{-14} ergs cm ⁻³) * | $3.0 \pm 0.2 \pm 0.4$ | |
| B (μG) * | $0.87 \pm 0.03^{+0.05}_{-0.06}$ | |
| $u_{\text{e}}/u_{\text{m}}$ * | $1.1^{+0.2+0.4}_{-0.1-0.2}$ | |

* The statistics from $S_{1\text{keV}}$ is propagated to the first error, while all the possible systematics are considered in the second one.

- Golombek, D., Miley, G. K., & Neugebauer, G., 1988, *AJ*, 95, 26
- Harris, D. E., & Grindlay, J. E., 1979, *MNRAS*, 188, 25
- Inoue, S. & Takahara, F., 1996, *ApJ*, 463 555,
- Ishisaki, Y., et al. 2007, *PASJ*, 59, 113
- Ishwara-Chandra, C. H., & Saikia, D. J., 1999, *MNRAS*, 309, 100
- Isobe, N., et al., 2002, *ApJ*, 580, L111
- Isobe, N., et al., 2009, *ApJ*, 706, 454
- Isobe, N., Makishima, K., Tashiro, M., & Hong, S., 2005, *ApJ*, 632, 781
- Isobe, N., Makishima, K., Tashiro, M., Itoh, K., Iyomoto, N., Takahashi, I., & Kaneda, H., 2006, *ApJ*, 645, 256
- Isobe, N., Seta, H., Gandhi, P., & Tashiro, M.S., 2011, *ApJ*, 727, 82
- Iyomoto, N., Makishima, K., Tashiro, M., Inoue, S., Kaneda, H., Matsumoto, Y., & Mizuno, T. 1998, *ApJ*, 503, L31
- Kalberla, P. M. W., Burton, W. B., Hartmann, Dap, Arnal, E. M., Bajaja, E., Morras, R., & Poëppel, W. G. L., 2005, *A&A*, 440, 775
- Kaneda, H., et al., 1995, *ApJ*, 453, L13
- Konar, C., Hardcastle, M. J., Croston, J. H., & Saikia, D. J. 2010, *MNRAS*, 400, 480
- Koyama K., et al., 2007, *PASJ*, 59, S23
- Kushino, A., Ishisaki, Y., Morita, U., Yamasaki, N. Y., Ishida, M., Ohashi, T., & Ueda, Y., 2002, *PASJ*, 54, 327
- Laing, R. A., Riley, J. M., & Longair, M. S. 1983, *MNRAS*, 204, 151
- Lumb, D. H., Warwick, R. S., Page, M., & De Luca, A., 2002, *A&A*, 389, 93
- Mack, K.-H., Klein, U., O’Dea, C.P., & Willis, A.G., 1997, *A&AS*, 123, 423
- Mewe, R., Gronenschild, E. H. B. M., & van den Oord, G. H. J. 1985, *A&AS*, 62, 197
- Mitsuda, K., et al., 2007, *PASJ*, 59, S1
- Rines, K., Geller, M. J., Diaferio, A., Mohr, J. J., & Wegner, G. A., 2000, *AJ*, 120, 2338
- Serlemitsos, P.J, et al., 2007, *PASJ*, 59, S9
- Schoenmakers, A. P., Mack, K.-H., de Bruyn, A. G., Röttgering, H. J. A., Klein, U., & van der Laan, H., 2000, *A&AS*, 146, 293
- Strom, R.G., Baker, J.R., & Willis, A.G., 1981, *A&A*, 100, 220
- Takahashi, T., et al., 2007, *PASJ*, 59, S35
- Takahashi, T., et al., 2010, *SPIE*, 7732, 27
- Tashiro, M., et al., 1998, *ApJ*, 499, 713
- Tashiro M., Isobe, N., Seta H., Yaji, Y., & Matsuta K., 2009, *PASJ*, 61, S327
- Tashiro, M., Makishima, K., Iyomoto, N., Isobe, N., & Kaneda, H., 2001, *ApJ*, 546, L19
- Tawa, N., et al., 2008, *PASJ*, 60, S11
- Uchiyama et al., 2008, *PASJ*, 60, S35
- Yaji, Y., et al., 2010, *ApJ*, 714, 37